

ACCEPTED MANUSCRIPT

Cross-correlation analysis of pulse wave propagation in arteries: *in vitro* validation and *in vivo* feasibility

To cite this article before publication: Pierre Nauleau *et al* 2018 *Phys. Med. Biol.* in press <https://doi.org/10.1088/1361-6560/aabe57>

Manuscript version: Accepted Manuscript

Accepted Manuscript is “the version of the article accepted for publication including all changes made as a result of the peer review process, and which may also include the addition to the article by IOP Publishing of a header, an article ID, a cover sheet and/or an ‘Accepted Manuscript’ watermark, but excluding any other editing, typesetting or other changes made by IOP Publishing and/or its licensors”

This Accepted Manuscript is © 2018 Institute of Physics and Engineering in Medicine.

During the embargo period (the 12 month period from the publication of the Version of Record of this article), the Accepted Manuscript is fully protected by copyright and cannot be reused or reposted elsewhere.

As the Version of Record of this article is going to be / has been published on a subscription basis, this Accepted Manuscript is available for reuse under a CC BY-NC-ND 3.0 licence after the 12 month embargo period.

After the embargo period, everyone is permitted to use copy and redistribute this article for non-commercial purposes only, provided that they adhere to all the terms of the licence <https://creativecommons.org/licenses/by-nc-nd/3.0>

Although reasonable endeavours have been taken to obtain all necessary permissions from third parties to include their copyrighted content within this article, their full citation and copyright line may not be present in this Accepted Manuscript version. Before using any content from this article, please refer to the Version of Record on IOPscience once published for full citation and copyright details, as permissions will likely be required. All third party content is fully copyright protected, unless specifically stated otherwise in the figure caption in the Version of Record.

View the [article online](#) for updates and enhancements.

Cross-correlation analysis of pulse wave propagation in arteries: *in vitro* validation and *in vivo* feasibility

Pierre Nauleau¹, Iason Apostolakis¹, Matthew McGarry¹, Elisa Konofagou^{1,2}

¹ Department of Biomedical Engineering, Columbia University, New York, NY, USA

² Department of Radiology, Columbia University, New York, NY, USA

E-mail: ek2191@columbia.edu

Abstract. The stiffness of the arteries is known to be an indicator of the progression of various cardiovascular diseases. Clinically, the pulse wave velocity (PWV) is used as a surrogate for the arterial stiffness. Pulse Wave Imaging (PWI) is a non-invasive, ultrasound-based imaging technique capable of mapping the motion of the vessel walls allowing local assessment of the arterial properties. Conventionally, a distinctive feature of the displacement wave (e.g. the 50% upstroke) is tracked across the map to estimate the PWV. However, the presence of reflections, such as those generated at the carotid bifurcation, can bias the PWV estimation. In this paper, we propose a two-step cross-correlation based methods to characterize arteries using the information available in the PWI spatio-temporal map. First, the area under the cross-correlation curve is proposed as an index to locate regions of different properties. Second, a local peak of the cross-correlation function is tracked to obtain a less biased estimate of PWV. Three series of experiments were conducted in phantoms to evaluate the capabilities of the proposed method and compare it against the conventional method. In the ideal case of a homogeneous phantom, the two methods performed similarly and estimated correctly the PWV. In the presence of reflections, the proposed method provided a more accurate estimate than the conventional processing: e.g for the soft phantom, biases of -0.27 and $-0.71 \text{ m} \cdot \text{s}^{-1}$ were observed. In a third series of experiments, the correlation-based method was able to locate, with an error smaller than 1 mm, two regions of different properties. It also provided more accurate PWV estimates than the conventional processing (biases: -0.12 vs $-0.26 \text{ m} \cdot \text{s}^{-1}$). Finally, *in vivo* feasibility of the proposed method was demonstrated in eleven healthy subjects. The results indicated that the correlation-based method might be less precise *in vivo* but more accurate than the conventional method.

PACS numbers: 8170Cv, 8785Ng

Submitted to: *Phys. Med. Biol.*

*Cross-correlation analysis of pulse wave propagation in arteries: in vitro validation and in vivo feasibility2***1. Introduction**

Cardiovascular disease (CVD) has been recognized as the leading cause of death worldwide (Roth et al. 2015). The stiffness of arteries has been associated with a large range of CVD (Messas et al. 2013) such as hypertension (Safar et al. 2003) and atherosclerosis (de Korte et al. 2011). Changes in arterial stiffness reflect the progression of disease and can serve as an index of morbidity or mortality (Zieman et al. 2005). Therefore, accurate measurements of the arterial stiffness could help to define the risk of cardiovascular events and enable early intervention. Clinically, arterial stiffness can be observed through Pulse Wave Velocity (PWV) (Willum-Hansen et al. 2006), (Vappou et al. 2010). The pulse wave refers to the pressure and flow velocity waves generated by the contraction of the left ventricle of the heart. This wave propagates through the arterial tree and induces displacements of the vascular walls. The current clinical method estimates the PWV based on the propagation time of the arterial pulse between the common carotid and the femoral arteries. It thus yields an average PWV value for the entire region. However, CVD is known to regionally modify the arteries: for example, a stronger spatial variation in the distensibility of the carotid has been shown in hypertensive patients compared to healthy subjects (Reneman et al. 2005). Several research teams are developing non-invasive ultrasound methods to locally assess the properties of the arteries using shear-wave imaging (Couade et al. 2010), acoustic radiation force impulse imaging (Behler et al. 2008) and Pulse Wave Imaging (PWI). The PWI method is based on a motion tracking algorithm (Luo & Konofagou 2010) to measure the displacements of the vessel walls in order to map the propagation of the pulse wave (Vappou et al. 2010). Conventionally, the propagation of the wave is quantified by tracking a feature for each displacement waveform observed by the multi-element probe. A previous study has evidenced that the 50% upstroke provided the most precise and uniform measurement of PWV *in vivo* (Li et al. 2015). A linear model is fitted to the spatio-temporal data to estimate the PWV, locally, across the field of view. The method was recently adapted to estimate PWV at smaller scales using a sliding kernel with fixed size and overlap percentage, a method called piecewise Pulse Wave Imaging (Apostolakis et al. 2016). However, these techniques only use one marker per recorded waveform (i.e., the 50% upstroke) while the entire displacement wavelet (typically 2000 samples for each recording), carrying rich information on the arterial mechanical properties is available. Moreover, the presence of a reflected wave in the field of view can modify the pulse wave profile and hence bias the estimation of PWV (McGarry et al. 2016). Reflections occur for example at the carotid bifurcation. These issues can be addressed by using the calculated wall displacements as an input of an inverse problem (McGarry et al. 2016).

In this paper, we present an alternative method, based on the cross-correlation principle, to address the aforementioned limitations at a lower computational cost. First, the proposed cross-correlation based method is described. The capabilities of the proposed technique are evaluated in phantoms. Finally, *in vivo* feasibility is tested.

2. Materials and Methods

2.1. Rationale for the use of cross-correlation characterization

The cross-correlation is an operation that quantifies the similarity between two signals, $f(t)$ and $g(t)$, as a function of the delay of one relatively to the other, t_{Corr} . It is defined mathematically as follows

$$(f \star g)(t_{Corr}) = \int_{-\infty}^{\infty} f^*(t)g(t + t_{Corr})dt,$$

where f^* denotes the complex conjugate of f .

A common application of cross-correlation is the estimation of a delay between two similar signals. The position of the maximum of the cross-correlation function indicates the time point for which the signals are best aligned. The value of the maximum characterizes the similarity of the two studied signals. We propose to use these two tools (value and position of the maximum) to analyze the propagation of the pulse wave across the ultrasonic array.

If a wave is propagating from A to B with a speed c , the cross-correlation function of the signals observed in A and B will produce a packet centered around $\tau = \frac{d_{AB}}{c}$. If two waves are propagating in opposite directions with respective speeds c_F and c_R (these two speeds being equal in most of the common situations), the correlation function will produce four packets corresponding to the interaction between: i) the forward wave observed in A and the forward wave observed in B, ii) the forward wave observed in A and the reflected wave observed in B, iii) the reflected wave observed in A and the forward wave observed in B, iv) the reflected wave observed in A and the reflected wave observed in B. These four packets are centered around

$$\begin{cases} \tau_i = t_{FA} - t_{FB} = \frac{d_{AB}}{c_F} \\ \tau_{ii} = t_{FA} - t_{RB} = (t_{FA} - t_{RA}) + \frac{d_{AB}}{c_R} \\ \tau_{iii} = t_{RA} - t_{FB} = (t_{RA} - t_{FA}) + \frac{d_{AB}}{c_F} \\ \tau_{iv} = t_{RA} - t_{RB} = \frac{d_{AB}}{c_R} \end{cases} \quad (1)$$

t_{FA} (resp. t_{RA}) being the time of arrival of the forward wave (resp. reflected wave) in A and t_{FB} (resp. t_{RB}) being the time of arrival of the forward wave (resp. reflected wave) in B. The shapes, number of peaks and amplitudes of the four different packets depend on the shape, number of peaks and amplitudes of the signals of interest, observed in A and B. An example illustrating the presence of the four packets for two ideal signals is provided in figure 1.

2.2. Phantom manufacturing

Room-temperature vulcanizing silicone gels were chosen for their long-lasting properties to form a vessel phantom with two parts of different mechanical properties (McGarry et al. 2016). A two-part custom mold was 3D-printed in polylactic acid (PLA)

Cross-correlation analysis of pulse wave propagation in arteries: *in vitro* validation and *in vivo* feasibility⁴

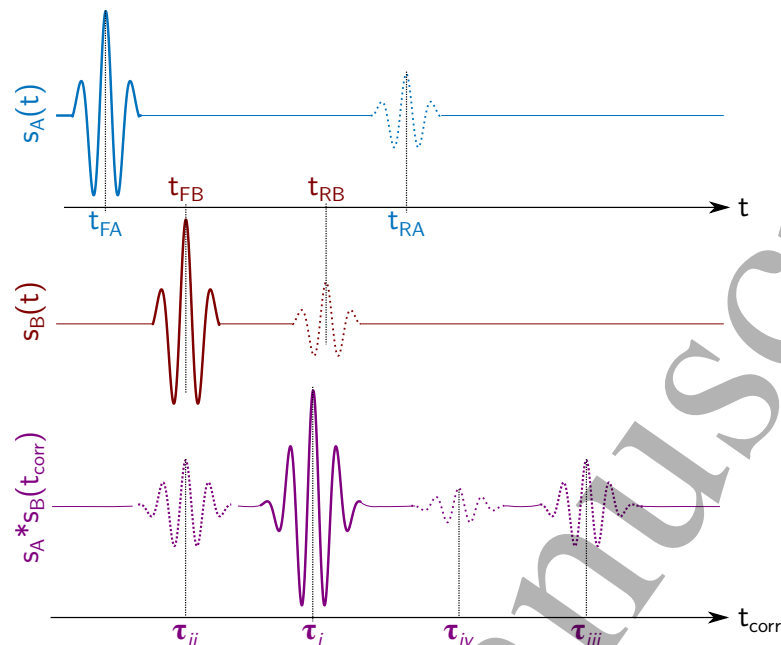


Figure 1. Example illustrating the four packets observed in the cross-correlation function (bottom row) of two signals: $s_A(t)$ (top row) and $s_B(t)$ (middle row) containing a forward-propagating wave (bold line, labelled FA and FB) and a reflected wave (dotted line, labelled RA and RB).

(MakerBot, NY, USA). The mold is a 240 mm-long cylinder with an internal diameter of 14 mm. A 8 mm-diameter acrylic rod was used to generate the lumen. The dimensions of the phantom were chosen for ease of manufacture. The material for the softer part of the phantom was 100% A341 silicone gel (Factor II, Lakeside, AZ, USA) and the one for the stiffer part was 70% A341 and 30% LSR-05 silicone elastomer (Factor II, Lakeside, AZ, USA). Two different concentrations of scatterers (corn starch powder) were used to distinguish the two parts on the ultrasonic images: $25 \text{ g} \cdot \text{L}^{-1}$ for the soft vs. $125 \text{ g} \cdot \text{L}^{-1}$ for the stiff. After mixing, the solutions were vacuum degassed to prevent the formation of air bubbles. The mold and the central rod were coated with petroleum jelly to ease the future extraction of the phantoms. With the mold held vertically, half of it was filled with the soft material poured with a syringe. After about an hour of curing, the stiff material was poured on top of the soft layer. When curing, the two parts naturally adhere to each other. Finally, the mold was opened and extra petroleum jelly was used to completely extract the phantom. A schematic representation of the resulting phantom is shown in figure 2. It was mounted on plastic fittings in a container. Pre-stretch was applied to keep the phantom straight. The phantom was embedded in a soft silicone background made from 40% A341 gel and 60% Xiameter PMX-200 100CS silicone fluid (Dow Corning, Midland, MI, USA). The vessel lumen was then filled with water.

The considered-true value of PWV in each part of the phantom was characterized through static testing. While the pressure was varied using water columns of heights

Cross-correlation analysis of pulse wave propagation in arteries: *in vitro* validation and *in vivo* feasibility

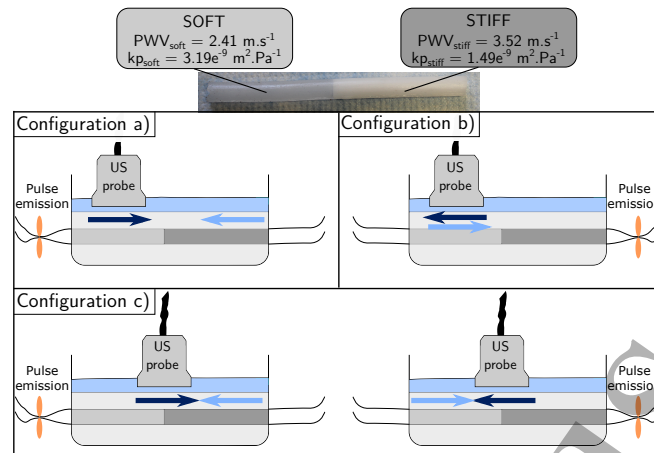


Figure 2. Three experimental configurations investigated on a phantom with two parts of different scatterer concentration and stiffnesses: a) ideal conditions: an homogeneous part (either soft or stiff) was imaged with little influence from the reflection at the outlet fitting (light blue arrow) by emitting a wave (dark blue arrow) on the side close to the probe, b) an homogeneous part (either soft or stiff) was imaged with strong influence from the reflection, c) the transition between the soft and the stiff parts was imaged with emission on each side successively.

ranging from 0 to 150 mm, in steps of 10 mm, the diameter of the phantom lumen was measured on ultrasound images with a semi-automated segmentation software. The segmentation algorithm detects the sharp transition between the lumen (containing no scatterers) and the phantom walls (containing a lot of scatterers). Within this pressure range, the relationship between the radius, r , and the pressure, P , was considered linear:

$$r = r_0 + k_{pr}P. \quad (2)$$

k_{pr} was estimated by a linear fit of the measurements. k_p , the vessel compliance, was then calculated as follows (Reneman et al. 1986)

$$k_p = 2\pi r k_{pr}. \quad (3)$$

The gold standard for PWV, PWV_{true} , was then computed from k_p using the Bramwell-Hill equation (Bramwell & Hill 1922):

$$PWV_{true} = \sqrt{\frac{A}{k_p \rho}}, \quad (4)$$

where A is the cross-sectional area of the vessel and ρ the density of the fluid in the lumen. The properties were calculated at each point of the longitudinal cross-section of the phantom. The values obtained within a presumed homogeneous region (either the soft one or the stiff) were averaged (mean value and standard deviation were calculated). The stiff part of the phantom was found to be approximately twice less compliant than the soft part ($1.49e^{-9} \text{ m}^2 \cdot \text{Pa}^{-1}$ vs. $3.19e^{-9} \text{ m}^2 \cdot \text{Pa}^{-1}$). The corresponding velocities ($PWV_{stiff} = 3.52 \pm 0.19 \text{ m} \cdot \text{s}^{-1}$ and $PWV_{soft} = 2.41 \pm 0.31 \text{ m} \cdot \text{s}^{-1}$) were within the range of those observed *in vivo* (Luo et al. 2012). The standard deviations for static

Cross-correlation analysis of pulse wave propagation in arteries: in vitro validation and in vivo feasibility

testing reflect the inhomogeneity of the phantom as well as errors in the estimation of the cross-section area.

2.3. Validation experiments in phantom

Three configurations of experiment were investigated with this phantom. A single pulse excitation (generated by releasing the inlet pipe) was chosen rather than continuous excitation with a peristaltic pump to avoid the presence of waves bouncing back and forth between the two sides of the phantom and affecting the PWV measurements. In configuration a (figure 2 (a)), an homogeneous part of the phantom was imaged (either the soft or the stiff) and a single pulse was emitted on the side located closer to the site of imaging. The measurements were thus only slightly affected by reflections from the fitting. In configuration b (figure 2 (b)), the same part was imaged but the pulse was emitted on the opposite side. In this case, the measurements were strongly affected due to the proximity to the reflection site (i.e., the outlet fitting on the left). In configuration c (figure 2 (c)), the transition between the soft part and the stiff part was imaged. The imaged part being approximately equally distant from both reflection sites, the influence of the reflections should be similar if the pulse comes from the left or right side. Each experiment was repeated five times. Hence, the configurations a and b consists of five experiments for the soft part, five experiments for the stiff part and the configuration c of ten experiments.

In order to evaluate the accuracy of the proposed method in locating a transition in the vessel material properties, the experiments in configuration c were repeated after having moved the probe twice, by a controlled distance (6.35 mm) in the longitudinal direction, towards the soft part of the phantom.

The capabilities of the two methods in these phantom experiments were compared based on the biases between the estimated PWV and the true value, obtained with static testing. For each experimental configuration, the difference between the PWV estimates obtained from conventional processing and the true value obtained by static testing on one hand and the PWV estimates obtained from correlation-based processing and the true value on the other hand were calculated. The mean difference and the standard deviation (or median and percentiles for non-normally distributed data) of the differences enable the bias and the limits of agreement (mean $\pm 1.96 \times$ standard deviation) between the method and the gold standard to be quantified.

2.4. In vivo feasibility

The common right carotid of eleven healthy subjects was imaged with the ultrasound system described in the next section for two different studies. These two studies were approved by the Institutional Review Board of Columbia University. Informed consent has been received from every subject.

Cross-correlation analysis of pulse wave propagation in arteries: *in vitro* validation and *in vivo* feasibility

The first study was conducted with five subjects aged 22 to 32 years old (25.8 ± 4.5 y.o) to compare the precision of the two methods. The experiments were conducted with the subject sitting in a chair, freely breathing. The location of the carotid bifurcation was first determined using the ultrasound real-time B-mode images. Then, the probe was moved about 20 mm below the bifurcation to perform the acquisition. The exact distance between the bifurcation and the site of imaging was measured with a mechanical caliper. The imaging sequence was repeated five times with repositioning of the probe and movements of the subject between acquisitions.

The second study was conducted with six subjects to investigate the influence of the location of the acquisition on the PWV estimates. The common right carotid of those subjects was imaged at three different locations along the longitudinal axis. The subjects were 25 to 37 years old, with an average age of 30.3 y.o. The first acquisition was performed with the probe located so that the carotid bulge would appear at the border of the field of view. For the second and third acquisitions, the probe was moved along the longitudinal axis by respectively, 16.24 and 28.30 mm in average.

No gold standard was available for this *in vivo* feasibility study. For the first series of experiments, the PWV estimated by each method were compared for each subject using median and 25th and 75th percentile. A Wilcoxon signed-rank test was used to do a paired comparison between the PWV estimated by each method. For the second series, the bias between the PWV estimated by the conventional technique and the PWV estimated by the cross-correlation method was calculated for each subject, in each position. Median, 25th and 75th percentile were used to compare the biases for each position. A Wilcoxon signed-rank test was used to do a paired comparison of those calculated biases between the different positions.

2.5. Ultrasound acquisition system

The RF data corresponding to the backscattered signals in the phantom and *in vivo* experiments were acquired using a research echographic scanner (Vantage, Verasonics Inc., Redmond, WA, USA). The probe was a 5 MHz linear array, used in clinics for carotid imaging (ATL L7-4, ATL Ultrasound, Bothell, WA, USA). The 128 elements of this array cover a field of view of 37.6 mm.

Compound imaging sequences were used to achieve a high frame rate without trading off the data quality (Tanter & Fink 2014), (Apostolakis et al. 2017). The studied medium was insonified with 3 plane waves at angles of $[-10^\circ, 0^\circ, 10^\circ]$ for the phantoms, and 5 planes waves at angles of $[-10^\circ, -5^\circ, 0^\circ, 5^\circ, 10^\circ]$ for the *in vivo* acquisitions. The frame rates achieved were respectively 2600 fps and 1600 fps for the phantom and the healthy subject acquisitions. These frame rates are high enough to allow for an accurate observation of the pulse wave propagation (Apostolakis et al. 2017). The RF signals were recorded during 1 s and digitized at 20 MHz.

Parallel beamforming with a graphical processing unit-based computer was used to

Cross-correlation analysis of pulse wave propagation in arteries: in vitro validation and in vivo feasibility

reconstruct one series of frames from the 3 (for the phantom) or 5 (for the *in vivo* experiments) series of frames acquired. With a graphical processing unit NVIDIA Tesla C2075 and 48 GB of memory, this operation typically takes 5 min.

2.6. Pulse Wave Imaging

The PWI technique has previously been developed by our group (Fujikura et al. 2007), (Luo & Konofagou 2010), (Luo et al. 2012), (Li et al. 2015).

The acquired and beamformed RF data are processed with a fast 1D cross-correlation algorithm (Luo & Konofagou 2010) to estimate the incremental axial displacements of the vascular tissues. The anterior and the posterior walls of the vessel (or phantom) are manually segmented on the images. The walls are tracked across different frames. The propagation of the pulse wave is visualized by plotting the displacements of the walls coded in color, over time, along the path of propagation in the longitudinal direction. These images are called spatio-temporal maps and are the data analyzed in the PWV estimation process.

In order to filter out any rigid motion and to reduce the noise, the spatio-temporal map of the posterior wall was subtracted from the anterior wall spatio-temporal map, i.e., the distension of the artery was tracked (Meinders et al. 2001).

2.7. Conventional estimation of the PWV

Conventionally, to analyze the spatio-temporal map of the propagation, a distinctive feature of the pulse wave (e.g. the peak or the 50% upstroke) was tracked across the field of view, for each line of the map. A linear fit was performed between the time of arrival of this feature and the traveled distance. The slope of this fit yields a PWV estimate, while the coefficient of determination, r^2 , indicates the quality of the fit.

2.8. Correlation-based detection of a transition

The purpose of the method presented in this paper is to make better use of the information available in the spatio-temporal map.

First, we propose to use a correlation-based index to locate areas of different properties in the field of view. When propagating within a plaque rather than in a normal part of the carotid or in a stiffer part of the phantom, the pulse wave is attenuated and distorted. This can be seen qualitatively in the spatio-temporal map. The correlation function characterizing the similarity of two signals (in this case, the distension curves at two different positions along the longitudinal direction), it could quantify such alterations. We propose to calculate the cross-correlation functions between one reference line and all the subsequent lines of the spatio-temporal map and to use the area under

Cross-correlation analysis of pulse wave propagation in arteries: *in vitro* validation and *in vivo* feasibility

the normalized curve of correlation as an index of similarity. The normalization consists in dividing the correlation function between the distension curves at longitudinal position i and position j by the maximum of this correlation function. The area under each cross-correlation curve is estimated using a trapeze approximation. The evolution of this index across the vessel/phantom indicates the areas with different properties in the field of view. A transition was defined quantitatively based on the maximum of the first derivative of the AUC index.

2.9. Correlation-based estimation of the PWV

Correlation is then used to estimate the PWV in each of the previously identified areas of the spatio-temporal map. Let us consider that the first of these areas represents N_h lines of the spatio-temporal map. A correlation map is generated by calculating the cross-correlation function between the distension curve at the first position and the distension curves at all the other $N_h - 1$ positions and using a color code for the amplitude of the correlation function (figure 3). This process is repeated using each of the N_h lines of the spatio-temporal map successively as the reference signal. N_h cross-correlation maps are thus created.

Each of those maps presents one main peak around $t_{Corr} = 0$ s and a certain number of secondary peaks. As indicated in Rationale, these secondary peaks can be separated in four packets associated with the interaction of the forward and reflected waves. Two of these packets propagate with the velocity of the forward wave while the two other ones propagate with the velocity of the reflected wave, see (1). Tracking their peaks across the correlation map is thus a means of estimating the PWV.

In this application, due to the shape and speed of the pulse wave, the forward and reflected waves are mixed and the different packets of the correlation maps tend to merge. The central packets (τ_i and τ_{iv} in the rationale section) propagates in opposite directions toward each other. The merging of two packets will then be more important in the central part of the correlation maps. On the other hand, the side packets (τ_{ii} and τ_{iii} in the rationale section) propagates in opposite directions but further away from the central packets (resp τ_i and τ_{iv}). These side packets (and especially the peak of these packets located further from the center of the map $t_{Corr} = 0$) will be less affected by the merging of the forward and reflected waves. Therefore, to get an estimate unbiased by the presence of reflected waves, we propose to track the most distant peak (which is the least affected by the reflections) instead of tracking the central peak of the correlation map. For each correlation map, all the peaks are extracted (using existing Matlab functions) and the most distant one is tracked across the field of view (black squares). The arrival times of this peak, less biased by reflections, are fitted to a line (red line), which yields a PWV estimate. The tracking and fitting operations are repeated for each of the N_h correlation maps. The N_h PWV estimates are averaged to yield the final estimate value (figure 3). This entire process is repeated for each of the areas previously identified.

Cross-correlation analysis of pulse wave propagation in arteries: *in vitro* validation and *in vivo* feasibility

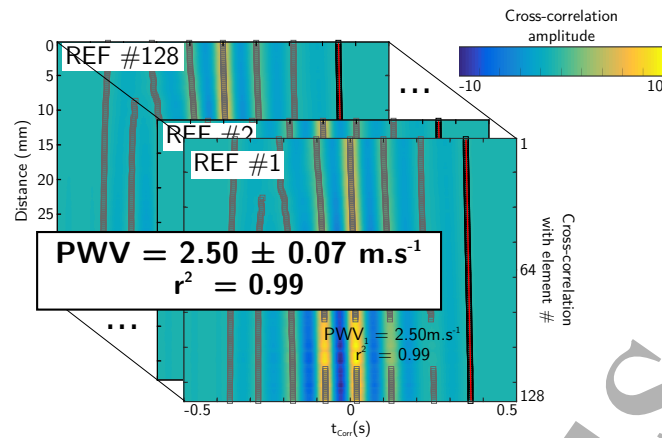


Figure 3. Each map represents the correlation functions between a reference line and all the other lines of a spatio-temporal map, coded in color. On each map, the peak located at the highest abscissa (shown to be less affected by reflections) is tracked across the field of view. A linear fitting yields a PWV estimate for each correlation map ($2.50 \text{ m} \cdot \text{s}^{-1}$ for the first map). These different PWV are averaged to obtain the PWV estimate ($2.50 \pm 0.07 \text{ m} \cdot \text{s}^{-1}$) for this experiment.

273

274 3. Results

275 3.1. Validation experiments in phantom

276 The propagation observed for the three experimental configurations are depicted in the
 277 spatio-temporal maps of the figure 4. Conventional processing was applied to these
 278 maps. In configuration a, the alignment of the wave peaks along a straight line indicate
 279 that a forward wave is propagating unaffected by reflections (figure 4 a)). This is ex-
 280 pected due to the proximity between the measurement and the reflection sites. The esti-
 281 mated PWVs (2.70 and $2.23 \text{ m} \cdot \text{s}^{-1}$ for the conventional and correlation-based processing
 282 respectively) approximates the true value ($2.41 \text{ m} \cdot \text{s}^{-1}$). Conversely, the curved profile
 283 observed in configuration b depicts the presence of a reflected wave which interferes with
 284 the forward propagating wave after a distance of 25 mm (figure 4 (b)). The reflected wave
 285 is responsible for the underestimation of the PWV ($1.62 \text{ m} \cdot \text{s}^{-1}$) by the conventional pro-
 286 cessing compared to the correlation-based estimate ($2.16 \text{ m} \cdot \text{s}^{-1}$). In configuration c, the
 287 spatio-temporal map obtained at the transition between the soft (top) and the stiff part
 288 (bottom) shows the alterations of the pulse wave when propagating through regions of
 289 different properties (figure 4 (c)). However, the conventional processing does not detect
 290 this difference: a single PWV can be estimated for the whole field of view with a good r^2
 291 (in average for the ten experiments, ($PWV = 3.24 \pm 0.46 \text{ m} \cdot \text{s}^{-1}$, $r^2 = 0.94 \pm 0.05$). The
 292 area under the correlation curve was first used to detect the transition, the conventional
 293 processing was then applied separately to the two areas. As indicated in figure 4 c,
 294 the conventional processing leads to a misclassification: the soft region is estimated to

294

60

Cross-correlation analysis of pulse wave propagation in arteries: *in vitro* validation and *in vivo* feasibility

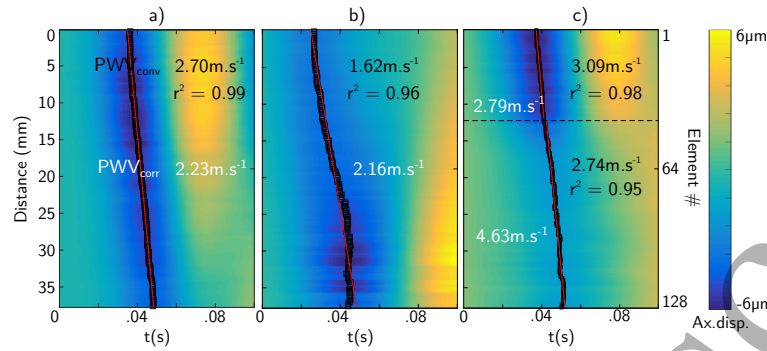


Figure 4. Examples of spatio-temporal maps obtained for each configuration: for homogeneous soft phantom a) under ideal conditions, b) in the presence of a strong reflection, and, c) for a bi-phasic phantom, the softer part being on the top of the map. The indicated PWV have been estimated by conventional processing (linear fitting in red of the 50% upstroke markers in black). The true PWV values are $PWV_{soft} = 2.41 \text{ m} \cdot \text{s}^{-1}$ and $PWV_{stiff} = 3.52 \text{ m} \cdot \text{s}^{-1}$.

present higher PWV ($3.09 \text{ m} \cdot \text{s}^{-1}$) than the stiff region ($2.74 \text{ m} \cdot \text{s}^{-1}$). The correlation-based method provides a more accurate characterization of the two regions: 2.79 vs. $4.63 \text{ m} \cdot \text{s}^{-1}$.

For each experiment, the first line of the spatio-temporal map was used as a reference to calculate the area under the correlation curve index (figure 5). For the configurations a and b where the homogeneous part of the phantom was imaged, the index remains fairly constant across the entire field of view. For the configuration c where the transition was imaged, the curve can be divided in two parts: a first part where the index evolves non monotonously and a second larger part where it remains constant. The configuration c experiments were repeated after moving twice the probe by 6.35 mm. Using the derivative of the AUC index, the transition was estimated at locations separated respectively by 5.40 and 6.00 mm (figure 6).

For the experiments performed under ideal conditions (configuration a), a small bias was observed for both the conventional processing ($0.09 \text{ m} \cdot \text{s}^{-1}$ for the soft part, $-0.80 \text{ m} \cdot \text{s}^{-1}$ for the stiff part) and the correlation-based processing ($0.10 \text{ m} \cdot \text{s}^{-1}$ for the soft part, $-0.49 \text{ m} \cdot \text{s}^{-1}$ for the stiff part) (figure 7). The interval between the limits of agreement is shorter for the correlation-based processing for the soft part (1.12 vs $2.20 \text{ m} \cdot \text{s}^{-1}$) and of similar size for the stiff part (1.57 vs $1.34 \text{ m} \cdot \text{s}^{-1}$).

For the experiments where reflections have more noticeable effects (configuration b), the conventional processing underestimates the PWV for the soft part (as observed previously in figure 4 (b)): a negative bias of $-0.71 \text{ m} \cdot \text{s}^{-1}$ is evidenced (figure 8). The correlation-based processing provides a less biased estimation since the bias is $-0.27 \text{ m} \cdot \text{s}^{-1}$. The interval between the limits of agreement is of similar size (0.62

Cross-correlation analysis of pulse wave propagation in arteries: *in vitro* validation and *in vivo* feasibility¹²

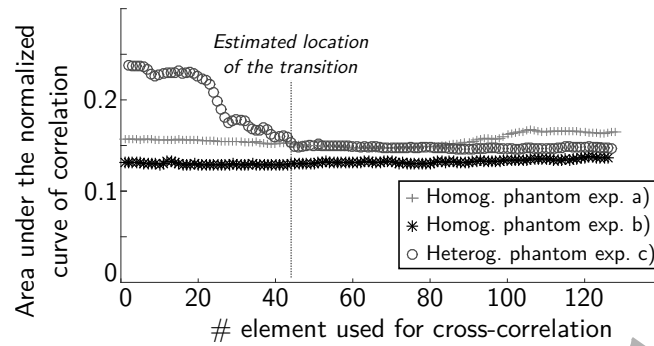


Figure 5. Examples of evolution of the AUC index for each experimental configuration. For the homogeneous phantom experiments, the index remains constant across the field of view. For the heterogeneous phantom, two phases can be identified and the location of the transition between the soft and the stiff parts can thus be estimated.

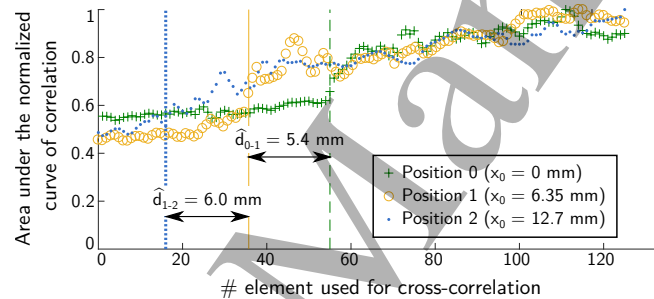


Figure 6. Evolution of the AUC index for three acquisitions of the transition between the soft and the stiff parts, the probe having been moved by 6.35 mm between acquisitions. Using the AUC index, the transition is estimated to have moved respectively by 5.40 and 6.00 mm between acquisitions.

for the conventional processing vs. $0.82 \text{ m} \cdot \text{s}^{-1}$ for the correlation-based analysis). For the stiff part, the conventional processing provided, in average, a value closer to the true value but the estimates were less reliable than the proposed correlation-based processing: the range of the limits of agreement is $2.70 \text{ m} \cdot \text{s}^{-1}$ for the conventional method vs $1.04 \text{ m} \cdot \text{s}^{-1}$ for the proposed method. The bias observed for the correlation-based method was consistent between the soft and the stiff experiments.

For the experiments of configuration c, we can first notice that both methods perform similarly for the transition soft to stiff compared to the transition stiff to soft (figure 9). The soft to stiff and stiff to soft results can then be combined for analysis. The average bias is larger for the conventional method ($-0.26 \text{ m} \cdot \text{s}^{-1}$) compared to the correlation-based method ($-0.12 \text{ m} \cdot \text{s}^{-1}$). Moreover, the biases plots indicate that the conventional processing does not correctly characterize the two parts of the phantom (figure 9). The four groups of estimates for the correlation-based method (figure 9 (b)) are scattered similarly around the mean bias, while the other plot (figure 9 (a)) indicates that the conventional processing consistently overestimates the PWV of the

Cross-correlation analysis of pulse wave propagation in arteries: *in vitro* validation and *in vivo* feasibility¹³

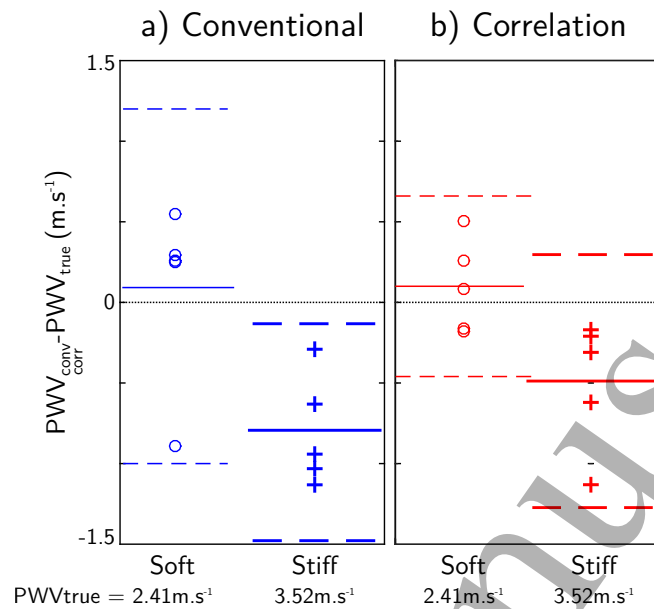


Figure 7. Differences between the PWV estimated by conventional processing with the gold standard, static testing method (a) and the PWV estimated by correlation-based processing with the same gold standard (b). Light lines and circles are related to the soft part, bold lines and crosses to the stiff part. Each of the circles (or crosses) represents one of the five experiments performed on the homogeneous phantom in ideal conditions (configuration a). The solid line indicates the bias while the dashed lines represent the limits of agreement.

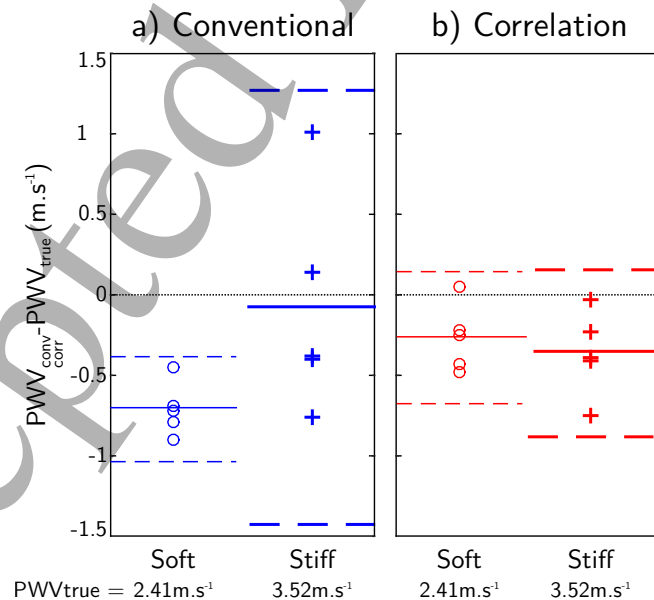


Figure 8. Differences between the PWV estimated by conventional processing with the gold standard, static testing method (a) and the PWV estimated by correlation-based processing with the same gold standard (b). Light lines and circles are related to the soft part, bold lines and crosses to the stiff part. Each of the circles (or crosses) represents one of the five experiments performed on the homogeneous phantom in presence of a strong reflection (configuration b). The solid line indicates the bias while the dashed lines represent the limits of agreement.

Cross-correlation analysis of pulse wave propagation in arteries: *in vitro* validation and *in vivo* feasibility

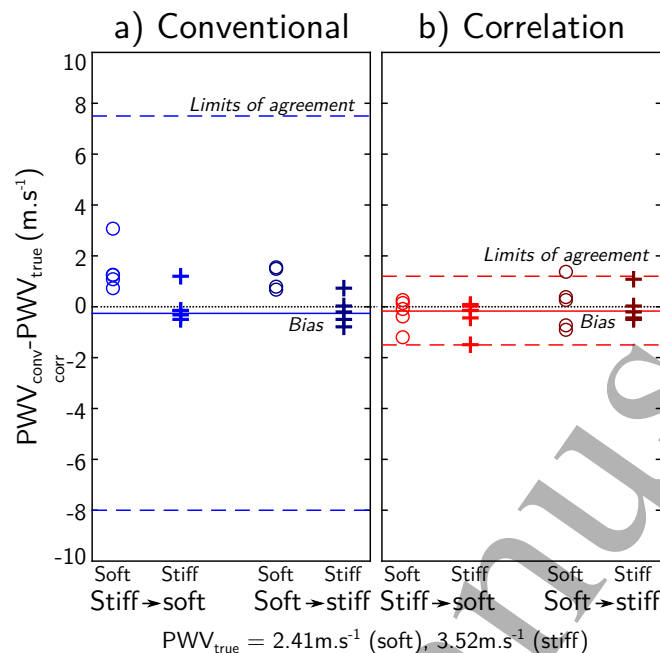


Figure 9. Differences between the PWV estimated by conventional processing with the gold standard, static testing method (a) and the PWV estimated by correlation-based processing with the same gold standard (b). The dark squares (resp. light crosses) depict the estimates obtained from the 10 experiments on the soft to stiff transition (resp. the stiff to soft transition) of an heterogeneous phantom (configuration c).

soft part and the estimates are in several cases higher than the estimates for the stiff part. The limits of agreement exhibit a much larger interval for the conventional than for the proposed processing (15.43 vs. $2.69 \text{ m} \cdot \text{s}^{-1}$) because of one specific experiment for which the soft part was wrongly estimated as $-14.09 \text{ m} \cdot \text{s}^{-1}$ by the conventional method while the correlation-based estimation yielded a more realistic estimate ($1.53 \text{ m} \cdot \text{s}^{-1}$).

3.2. *In vivo* feasibility

The distension wave pattern evolves noticeably along the propagation path, as shown in the spatio-temporal maps of a representative subject (figure 10). The V-shape pattern corresponding to the interference of the forward and the reflected waves is more or less visible depending on the proximity of the measurement site with the bifurcation. Close to the bifurcation, the two waves are merged in the almost entire field of view (figure 10 (a)). Far from the bifurcation, the forward wave is stronger and the V-shape is hardly visible (figure 10 (c)). Between these two extreme situations, the two waves are merged in the lower part of the map and distinct but of similar amplitude in the upper part (figure 10 (b)).

For each of the five subjects, the first line of the spatio-temporal map was used as

Cross-correlation analysis of pulse wave propagation in arteries: *in vitro* validation and *in vivo* feasibility¹⁵

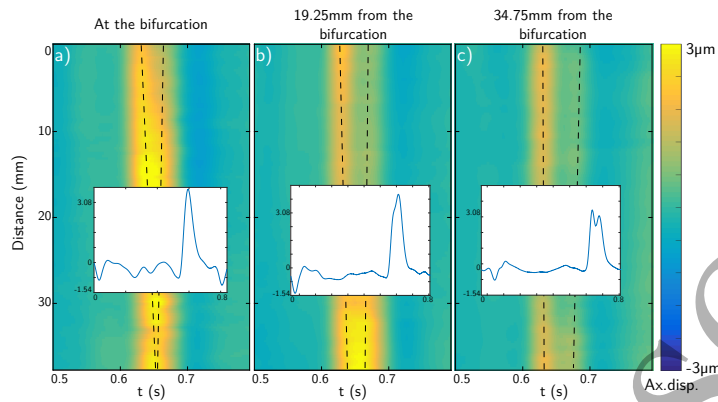


Figure 10. Examples of spatio-temporal maps showing the propagation of the displacement pulse wave in three different locations along the common carotid of a healthy subject. In each case, a forward wave and a reflected wave can be observed. Depending on the location of the measurement site, relatively to the carotid bifurcation, these two waves interfere more (close to the bifurcation) or less (far from the bifurcation). The inserts depict the waveform observed by the last element over a full cardiac cycle.

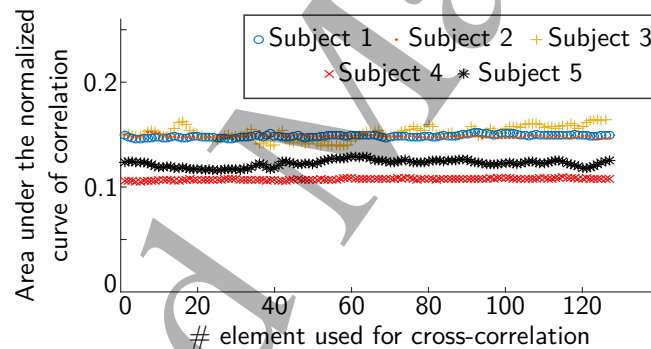


Figure 11. For each of the five healthy subjects, the evolution of the area under the curve of cross-correlation between a reference signal (first line of the spatio-temporal map) and the other lines indicates that the scanned part of the carotids consists of a single homogeneous region.

a reference to calculate the correlation function with all the other lines. A window of 0.3 to 0.5 ms centered around the main peak was used for the correlation. The proposed index, the area under the normalized curve of correlation remains relatively constant across the field of view, for each subject (figure 11).

The conventional processing and the proposed correlation-based processing methodologies were applied. The velocities obtained with the two methods are in the range of previously published values: $PWV_{conv} = 2.74 \pm 0.80 \text{ m} \cdot \text{s}^{-1}$ and $PWV_{corr} = 3.42 \pm 0.88 \text{ m} \cdot \text{s}^{-1}$ (Luo et al. 2012). For each subject, the two estimates are slightly different, the difference being significant only for subject 3 (figure 12).

The bias between the PWV estimated with each method was found to decrease when

Cross-correlation analysis of pulse wave propagation in arteries: *in vitro* validation and *in vivo* feasibility

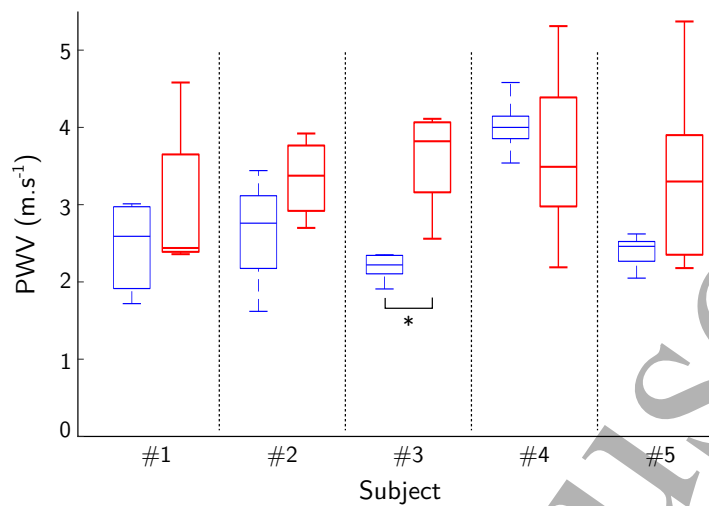


Figure 12. PWV estimates obtained with conventional processing (blue thin lines) and the correlation-based processing (red thick lines) in series of five acquisitions in five human carotids *in vivo*. Estimates are slightly but not significantly different between the methods, except for subject #3 ($p = 0.05$).

Table 1. Influence of the distance between the bifurcation, main source of reflections and the measurement site on the PWV estimates for both methods.

	Dist. from bifurcation (mm)	Bias ($\text{m} \cdot \text{s}^{-1}$)	Interquartile range ($\text{m} \cdot \text{s}^{-1}$)
Pos 1	0	1.01	1.04
Pos 2	16.24	0.84	0.54
Pos 3	28.30	0.79	1.68

367 moving away from the source of reflections, i.e. the bifurcation (table 1). However, the
 368 interquartile ranges were large and the observed trend was not statistically significant.

369 4. Discussion

370 In order to employ more of the information on the pulse wave propagation available
 371 from PWI, a new method based on the correlation study of the spatio-temporal map
 372 was validated in phantoms and feasibility was tested *in vivo*.

373
 374 The first part of the proposed method, the calculation of the AUC index, helps to
 375 identify regions of different properties: for homogeneous parts of the phantom, the index
 376 remained constant and for a field of view with different regions, a sudden variation of
 377 the index was observed, enabling us to locate the transition (figure 5). Quantitatively,
 378 the error in the transition location was evaluated by moving the probe by a controlled
 379 distance a couple of times. On the average, the location of the transition was estimated
 380 at 0.65 mm away from the actual location, which corresponds to an error of 10.24%.
 381 Therefore, this new index is relevant to accurately locate a transition in the vessel

properties.

This simple calculation provides additional information that could benefit other characterization methods such as the conventional PWV estimation or the Pulse Wave Inverse Problem (McGarry et al. 2016). In the experiments of configuration c, we demonstrate that the conventional processing indices (estimated PWV and fit quality r^2) do not accurately detect a transition: a good fit ($r^2 = 0.94 \pm 0.05$) was achieved despite the change in material properties. In the inverse problem method, the location of a transition or a reflection point would serve as an additional constraint in the problem and could then decrease the number of erroneous solutions.

The phantom experiments indicate that the proposed correlation-based method is more accurate than the conventional processing, especially in presence of reflections (figure 8) or when imaging the transition between a soft and stiff part (figure 9).

Under ideal conditions (configuration a), even though the two methods provided similar estimates (figure 7), the biases were higher for the stiff part than for the soft part. We hypothesize that this is due to the presence of reflections at the transition, these reflections being more present in the stiff part because of the higher speed of propagation.

When imaging the transition between the soft and stiff parts of the phantom (configuration c), the conventional processing overestimated the PWV of the soft part, independently of the direction of propagation (soft to stiff or stiff to soft), causing a misclassification of the regions. This bias is likely caused by the smaller size of the soft region compared to the stiff one in the field of view. Due to reduced number of 50% upstroke markers, the linear fit is less robust and more easily affected by noise. If we consider only the same number of lines/elements for the stiff area, an overestimation of the PWV was also observed (data not shown).

In vivo feasibility was shown in 11 healthy subjects.

In a first study with five patients, the constant AUC index indicated that the observed vessels were homogeneous. Considering that the subjects have normal arteries and that the images were taken far from the bifurcation (approximately 20 mm), this result was expected. As observed in figure 12, the PWV estimated by the correlation-based method exhibited a larger range than the conventional estimates. In other words, even though more accurate (as evidenced in the phantom studies), the correlation-based method is less precise than the conventional processing *in vivo*. In order to get a reliable estimate, it is thus mandatory to average the estimations resulting from different successive acquisitions on a same patient.

In the second study with six patients, for the acquisitions performed close to the bifurcation, the PWV was generally underestimated by the conventional methodology compared to the correlation-based method (a median bias of $1.01 \text{ m} \cdot \text{s}^{-1}$ was observed at the bifurcation). This observation is consistent with the results of the phantom study. Indeed, in this situation, due to the proximity with the bifurcation, the reflected waves

Cross-correlation analysis of pulse wave propagation in arteries: *in vitro* validation and *in vivo* feasibility

are more significant and the conventional processing was found to underestimate the PWV in presence of strong reflections. In addition, the observed bias was found to decrease, though non-significantly when moving away from the bifurcation. Therefore, we can conclude that the correlation-based method can provide a less biased estimation of the PWV *in vivo*.

An important parameter of the method is the location and length of the temporal portion of the spatio-temporal map used for the correlation-based analysis. This window should be short enough to correspond to a narrow pressure range). This window should also be long enough to contain both the direct and reflected waves, the proposed tracking would not otherwise be efficient. Indeed, the models (such as Moens-Korteweg or Bramwell-Hill) used to convert the PWV in an elasticity modulus depend on the pressure applied to the vessel, which varies through the cardiac cycle (i.e., through the spatio-temporal map).

The proposed method operates in the time domain: in the cases where the forward and the reflected waves are totally interfering, especially near sharp transitions, the correlation-based method will not be able to yield a truly unbiased estimation. The limit for which the unbiased estimation is possible depends on the temporal length, the velocity of the pulse wave and the proximity to the reflection site.

The method was proven feasible in eleven healthy human subjects. Clinical studies are now ongoing to evaluate the capability of the method to locate and characterize abnormal parts of the vessels in patients with atherosclerotic plaques.

5. Conclusion

A new processing technique of the PWI spatio-temporal maps was proposed. This method relies on the cross-correlation of the entire pulse waveforms to locate regions of different properties and estimate the PWV. Phantom studies evidenced that the proposed method provides a more accurate estimate than the conventional method. In a phantom, a transition between two regions was located with an error under 1 mm. The method was shown feasible in eleven healthy human subjects *in vivo*. The proposed method was found less precise than the conventional one, suggesting that averaging several successive acquisitions is mandatory to get a reliable PWV estimate.

Acknowledgments

Funding was provided in part by NIH R01HL135734.

Apostolakis, I. Z., McGarry, M. D., Bunting, E. A. & Konofagou, E. (2017). Pulse wave imaging using coherent compounding in phantoms and *in vivo*, *Physics in Medicine and Biology* **Accepted**.

*Cross-correlation analysis of pulse wave propagation in arteries: in vitro validation and in vivo feasibility*19

- 462 Apostolakis, I. Z., Nandlall, S. D. & Konofagou, E. E. (2016). Piecewise pulse wave imaging (ppwi) for
463 detection and monitoring of focal vascular disease in murine aortas and carotids in vivo, *IEEE*
464 *Transactions on Medical Imaging* **35**(1): 13–28.
- 465 Behler, R. H., Nichols, T. C., Zhu, H., Merricks, E. P. & Gallippi, C. M. (2008). Arfi imaging for
466 noninvasive material characterization of atherosclerosis part ii: Toward in vivo characterization,
467 *Ultrasound in medicine & biology* **35**(2): 278–295.
- 468 Bramwell, J. C. & Hill, A. V. (1922). The velocity of the pulse wave in man, *Proceedings of the Royal*
469 *Society of London B: Biological Sciences* **93**(652): 298–306.
- 470 Couade, M., Pernot, M., Prada, C., Messas, E., Emmerich, J., Bruneval, P., Criton, A., Fink, M.
471 & Tanter, M. (2010). Quantitative assessment of arterial wall biomechanical properties using
472 shear wave imaging, *Ultrasound in Medicine and Biology* **36**(10): 1662–1676.
- 473 de Korte, C. L., Hansen, H. H. G. & van der Steen, A. F. W. (2011). Vascular ultrasound for
474 atherosclerosis imaging, *Interface Focus* **1**(4): 565–575.
- 475 Fujikura, K., Luo, J., Gamarnik, V., Pernot, M., Fukumoto, R., Tilson, M. D. & Konofagou, E. E.
476 (2007). A novel noninvasive technique for pulse-wave imaging and characterization of clinically-
477 significant vascular mechanical properties in vivo, *Ultrasonic Imaging* **29**(3): 137–154.
- 478 Li, R. X., Qaqish, W. & Konofagou, E. E. (2015). Performance assessment of pulse wave imaging
479 using conventional ultrasound in canine aortas ex vivo and normal human arteries in vivo,
480 *Artery Research* **11**: 19 – 28.
- 481 Luo, J. & Konofagou, E. E. (2010). A fast normalized cross-correlation calculation method for
482 motion estimation, *IEEE Transactions on Ultrasonics, Ferroelectrics and Frequency Control*
483 **57**(6): 1347–1357.
- 484 Luo, J., Li, R. X. & Konofagou, E. E. (2012). Pulse Wave Imaging (PWI) of the human carotid artery:
485 an in vivo feasibility study, *The Journal of the Acoustical Society of America* **131**(4): 174–181.
- 486 McGarry, M., Li, R., Apostolakis, I., Nauleau, P. & Konofagou, E. E. (2016). An inverse approach to
487 determining spatially varying arterial compliance using ultrasound imaging, *Physics in Medicine*
488 *and Biology* **61**(15): 5486.
- 489 Meinders, J., Kornet, L., Brands, P. & Hoeks, A. (2001). Assessment of local pulse wave velocity in
490 arteries using 2-d distension waveforms., *Ultrasonic Imaging* **23**: 199–215.
- 491 Messas, E., Pernot, M. & Couade, M. (2013). Arterial wall elasticity: State of the art and future
492 prospects, *Diagnostic and Interventional Imaging* **94**(5): 561 – 569. Ultrasound elastography.
- 493 Reneman, R. S., Meinders, J. M. & Hoeks, A. P. G. (2005). Non-invasive ultrasound in arterial wall
494 dynamics in humans; what have we learned and what remains to be solved, *European Heart*
495 *Journal* **26**(10): 960–966.
- 496 Reneman, R., Van Merode, T., Hick, P., Muyltjens, A. & Hoeks, A. (1986). Age-related changes in
497 carotid artery wall properties in men, *Ultrasound in Medicine and Biology* **12**: 465–471.
- 498 Roth, G. A., Huffman, M. D., Moran, A. E., Feigin, V., Mensah, G. A., Naghavi, M. & Murray, C. J.
499 (2015). Global and regional patterns in cardiovascular mortality from 1990 to 2013, *Circulation*
500 **132**(17): 1667–1678.
- 501 Safar, M. E., Levy, B. I. & Struijker Boudier, H. A. J. (2003). Current perspectives on arterial stiffness
502 and pulse pressure in hypertension and cardiovascular diseases, *Circulation* **107**(22): 2864–2869.
- 503 Tanter, M. & Fink, M. (2014). Ultrafast imaging in biomedical ultrasound, *IEEE Transactions on*
504 *Ultrasonics, Ferroelectrics, and Frequency Control* **61**(1): 102–119.
- 505 Vappou, J., Luo, J. & Konofagou, E. E. (2010). Pulse wave imaging for noninvasive and quantitative
506 measurement of arterial stiffness in vivo., *American Journal of Hypertension* **23**(4): 393–398.
- 507 Willum-Hansen, T., Staessen, J. A., Torp-Pedersen, C., Rasmussen, S., Thijs, L., Ibsen, H. & Jeppesen,
508 J. r. (2006). Prognostic value of aortic pulse wave velocity as index of arterial stiffness in the
509 general population, *Circulation* **113**(5): 664–670.
- 510 Ziemann, S. J., Melenovsky, V. & Kass, D. A. (2005). Mechanisms, pathophysiology, and therapy of
511 arterial stiffness, *Arteriosclerosis, Thrombosis, and Vascular Biology* **25**(5): 932–943.